Observational constraint on cloud feedbacks suggests moderate climate sensitivity

Grégory V. Cesana[1,2*], Anthony D. Del Genio[2]

[1] Columbia University, Center for Climate Systems Research, Earth Institute, New York, NY
[2] NASA Goddard Institute for Space Studies, New York, NY.
[*] Correspondence to Gregory.cesana@columbia.edu

To submit to *Nature Climate Change*

Proposed editorial summary:

The response of low clouds to warming is uncertain among climate models and dominates spread in their projections. Satellite estimates of tropical cumulus and stratocumulus cloud feedbacks, derived using surface warming trends, suggest a more moderate climate sensitivity than many models predict.

Global climate models (GCMs) predict warming in response to increasing greenhouse gases, partly due to decreased tropical low-level cloud cover and reflectance. We use satellite observations that discriminate stratocumulus (Sc) from shallow cumulus (Cu) clouds to separately evaluate their sensitivity to warming and constrain the tropical contribution to low-cloud feedback. We find an observationally inferred low-level feedback two times smaller than a previous estimate. Cu are insensitive to warming whereas GCMs exhibit a large positive cloud feedback in Cu regions. In contrast, Sc show sensitivity to warming and the tropical inversion layer strength, controlled by the tropical Pacific SST gradient. Models fail to reproduce the historical SST gradient trends and therefore changes in inversion strength, generating an overestimate of the positive Sc cloud feedback. Continued weak east-Pacific warming would therefore produce a weaker low-cloud feedback and imply a more moderate climate sensitivity (3.47 ± 0.33 K) than many models predict.

When subjected to "external" forcings, such as anthropogenic changes in atmospheric greenhouse gases (GHGs), the atmosphere and surface warm at a rate determined not only by the forcing itself, but also by feedbacks, i.e., changes in other parts of the climate in response to the forcing, that either strengthen (positive feedback) or weaken (negative feedback) the warming. The most uncertain feedbacks are those due to changes in clouds, particularly low-altitude stratocumulus (Sc) and shallow cumulus (Cu) clouds over the oceans[1,2]. In response to surface warming, GCMs predict that low clouds primarily dissipate and amplify the warming by reflecting less solar radiation[1]. However, the range of low-cloud feedbacks simulated by individual climate models is diverse, varying from a small negative feedback to a large positive feedback[1]. In particular, the spread in tropical low-cloud feedback is the single biggest uncertainty in model's estimates of climate sensitivity[2–4], which explains the high correlation between the two quantities (Fig. 1f). Ultimately, this uncertainty limits our ability to project the magnitude of future climate change impacts.

Sc and Cu are driven by different cloud processes: cloud-top radiative cooling for Sc as opposed to surface convection for Cu[5]. In the tropics, Sc typically produce nearly overcast conditions off the west coasts of continents (Fig. 1a-c) and strongly reflect shortwave (SW) radiation back to space (Fig. 1b). Cu are more scattered and therefore have a smaller radiative effect (Fig. 1b). They are located in the extensive open ocean trade wind regions further west (Fig. 1a-c), Thus, there is no *a priori* reason to expect Sc and Cu to exhibit the same feedback in response to increasing GHGs. In GCMs, cloud feedback from regions dominated by Sc is comparable in strength to that in regions expected to be dominated by Cu or at the border between the two regimes (Fig. 1d)[1,3]. As a result, both regions contribute significantly to the difference in equilibrium climate sensitivity (ECS) between high-ECS and low-ECS models (Figs. 1e,f). A few multi-model studies have attempted to determine Sc or Cu cloud feedbacks, using fixed geographic areas[6] or large-scale conditions[7] as proxies to indirectly infer the presence of each cloud type, and found that the feedbacks are highly variable among models for both cloud types and roughly equally uncertain[8,9]. These studies, while intriguing, are limited because they do not robustly distinguish Cu and Sc clouds in GCM output and thus are not able to determine their respective feedbacks. Different feedbacks for Sc and Cu clouds are supported by idealized large-eddy simulation (LES) studies, yet understanding of the underlying reasons remains incomplete, particularly for trade-wind Cu[10], which may even produce negative feedbacks[11].

We use a new active remote sensing satellite product, the Cumulus and Stratocumulus CloudSat-Cloud-Aerosol Lidar and Infrared Pathfinder Satellite Observations (CALIPSO) Dataset (CASCCAD)[12], to explicitly identify Cu and Sc based on cloud morphology and altitude over 2007-2016. Simultaneous observations of the two primary local "cloud-controlling" environmental factors for Cu and Sc, i.e., sea surface temperature (SST) and estimated inversion strength (EIS)[13], are then used to estimate the change in low-cloud fraction[6,8] (LCC) for each cloud type in response to a change in global mean surface temperature (T).

$$\frac{dLCC}{dT} = \frac{\partial LCC}{\partial SST}\frac{dSST}{dT} + \frac{\partial LCC}{\partial EIS}\frac{dEIS}{dT} \quad (1)$$

Although other controlling factors[8] may affect low-cloud feedbacks[14], we do not consider them in the present study because their collective contribution to the low-cloud feedback is very small (see Supplementary Text 2 and Supplementary Fig. 4), consistent with previous findinds[8,14].

The partial derivatives ∂LCC/∂SST and ∂LCC/∂EIS can be calculated directly for Cu and Sc from CASCCAD over the decadal time span of the dataset and from a blend of observations and reanalysis products for SST and EIS (Supplementary Table 2). They are assumed to reflect fundamental local small-scale processes that regulate Cu and Sc and are thus invariant over different time scales[6,8]. The derivatives dSST/dT and dEIS/dT, on the other hand, indicate how the cloud-controlling environmental factors change as global mean surface temperature changes. These may be determined by large-scale processes associated with the tropical general circulation and may not be the same for different types of climate changes. In particular EIS should depend on changes in the large-scale tropical Walker circulation: a climate change that strengthens the SST gradient across the tropical Pacific Ocean should strengthen the Walker cell and increase EIS in the east Pacific Sc regions, while a change that weakens the gradient would weaken EIS instead[4]. Over the decadal period covered by CASCCAD, SST gradient changes are primarily due to El Niño and to a lesser extent the Pacific Decadal Oscillation, rather than anthropogenic climate change[15,16].

Cu-dominated regions cover a larger area of the tropics than Sc-dominated regions, but this is compensated by the greater cloud fraction in the Sc-dominated regions than in the Cu-dominated regions so that each type contributes a comparable amount to the total low cloud fraction (Figs. 1a,c, 2a). While the locations of Sc- and Cu-dominated regions can be roughly reproduced using a threshold on EIS –identified as a better Sc predictor than other environmental variables[13]– to discriminate Sc and Cu (Supplementary Fig. 2), it does not allow us to compute the correct total and partial derivatives of Sc and Cu cloud fractions as a function of the cloud-controlling variables SST and EIS (Supplementary Fig. 3), as well as their associated feedbacks (Supplementary Text 1). Despite the similar Sc and Cu cloud fractions, the observed response of low clouds to interannual local SST changes (i.e., the total derivative of LCC with respect to SST, dLCC/dSST, Eq. 2) is mainly controlled by Sc clouds in subsidence regimes over the tropical oceans (Fig. 2b).

$$\frac{dLCC}{dSST} = \frac{\partial LCC}{\partial SST} + \frac{\partial LCC}{\partial EIS}\frac{dEIS}{dSST} \qquad (2)$$

Sc cloud fraction largely decreases with local surface warming on interannual time scales (Fig. 2b), the result of a large decrease and increase of Sc cloud fraction with respect to SST and EIS (i.e., $\partial Sc/\partial SST$ and $\partial Sc/\partial EIS$, see Methods), respectively (Fig. 2c-d). On the contrary, in response to local surface warming, the Cu amount slightly increases (Fig. 2b), driven by its EIS component (Fig. 2d). Transition and other cloud types contribute relatively little to the total change (Supplementary Fig. 5).

These results provide an excellent test for GCMs, since they represent observed responses of specific cloud types to known SST changes that are routinely used to evaluate Coupled Model Intercomparison Project (CMIP) models. They do not reveal the long-term anthropogenic low-cloud feedback by themselves because interannual and interdecadal EIS changes may differ from long-term EIS changes[17]. Figures 2c-d do indicate, however, that the long-term low-cloud feedback is likely to be restricted primarily to the Sc regions, since $\partial Cu/\partial SST$ and $\partial Cu/\partial EIS$ are quite small. This conflicts with GCM projections that indicate a mostly large positive low-cloud feedback in the Cu regions[1,3] (Fig. 1d). One possible explanation for this model-observation discrepancy is the tendency for GCMs to create Sc-like artifact clouds at the base of Cu clouds, which are overly sensitive to changes in environmental conditions[18]. Another explanation is incorrect parameterized responses of Sc-Cu clouds to surface temperature and EIS changes[19].

Whether GCMs simulate the long-term anthropogenic low-cloud feedback correctly depends not only on their fidelity in parameterizing cloud processes, i.e., where Sc and Cu form and how they respond to cloud-controlling environmental factors, but also whether they correctly simulate the long-term evolution of the cross-Pacific SST gradient, which determines the evolution of EIS in the Sc regions[17]. For the past 20 to 30 years, the SST and EIS pattern trends have generated unusually small low-cloud feedbacks in the tropics[20,21] compared to that predicted by GCMs for long-term future climate. Recent studies argue that these pattern trends, which GCMs do not reproduce[15,22], are a manifestation of the natural variability and will not last in the coming decades. Instead, it has been argued that a weakening cross-Pacific SST gradient will emerge, leading to a strong positive low-cloud feedback[20,21,23]. However, we find that even on longer time scales (over the past 40 to 60 years), a time interval that should begin to incorporate some effects of anthropogenic GHG forcing, both the observed SST –in agreement with these previous studies[5]– and EIS patterns changes remain consistently different from the long-term changes predicted by the models (Fig. 3, Supplementary Fig. 6). Such a finding raises the question of how much weakening of the cross-Pacific SST gradient will actually occur in the future climate and what its ramification is for tropical low-cloud feedbacks.

Here we further quantify what could be the future SW low-cloud feedback should these past 40 to 60-year trends in SST and EIS (Fig. 3a-b-c-d) continue in the future. Previous studies have shown that the change in SW CRE is primarily driven by the change in LCC[6,8,14,19]. Consequently, the low-cloud feedback can be inferred by multiplying the change in LCC by the sensitivity of SW CRE to LCC[6,8,14] (i.e., $dCRE/dT = dCRE/dLCC\ dLCC/dT$), where the change in LCC is estimated from the sum of the partial derivatives of LCC with respect to controlling factors multiplied by the change in controlling factors (Eq. 1). Given the different responses of Sc and Cu to warming (Fig. 2), we further refine this method by computing separately the contributions from Sc and Cu clouds from the CASCCAD data ($dCRE_{Sc}/dT$ and $dCRE_{Cu}/dT$), weighting them as a function of their relative presence in a given location (i.e., Sc/(Sc+Cu) or Cu/(Sc+Cu)) and summing them to get the SW low-cloud feedback inferred from observations (dCRE/dT; see Eq. 4 in Methods).

Similarly, we also use the CASCCAD results to infer what would be the future SW low-cloud feedbacks should the SST and EIS patterns estimated from two future climate scenarios predicted by GCMs (Fig. 3e-f-g-h; abrupt-4xCO2 and uniform +4K; see Methods) really occur in the future.

These resulting estimated tropical low-cloud feedback, referred to as "observationally inferred" feedbacks, are shown in Fig. 4. If the SST and EIS pattern trends observed over the past 40 to 60 years continue in the coming decades, they will generate an observationally inferred SW low-cloud feedback up to two times smaller (Fig. 4a) than it would be if the future pattern trend resembles the pattern trend predicted by the CMIP6 models for an abrupt-4xCO2 climate warming scenario (Fig. 4g), and three times smaller than that of a hypothetical uniform +4K surface warming (Fig. 4j). By using the satellite dataset that is the most accurate for cloud-type discrimination and the most sensitive to Cu clouds, as well as by accounting for the spatial-dependence of the Sc and Cu partial derivatives as determined by the Sc/(Sc+Cu) fraction (Supplementary Fig. 8 and 9), our observationally inferred feedback estimate for an abrupt-4xCO2 SST and EIS pattern change scenario is 0.56 ± 0.15 $Wm^{-2}K^{-1}$ in subsidence regimes over the tropical oceans. Our result is two times smaller and with a five times narrower range than a previous multi-observational analysis estimate[8], which does not account for the different responses of Sc and Cu to warming and their relative presence in a given location (i.e., Sc/(Sc+Cu) fraction; Supplementary Fig. 10). The majority of this feedback is driven by Sc clouds in Sc-dominated regions regardless of the climate warming scenario (Fig. 4c-f-i-l and Supplementary Fig. 7c-f), contrary to previous belief[3,9,24,25], because (1) these Sc clouds are very sensitive to both surface warming and inversion strength, (2) Cu clouds are only weakly sensitive to inversion strength variations and are insensitive to surface warming (Supplementary Fig. 9), and (3) Sc clouds are less frequent in Cu-dominated regions than many GCMs simulate[18] (Fig. 1c).

Although a variety of cloud feedbacks exist (e.g., high-cloud and cloud phase-related optical-depth feedbacks), the SW low-cloud feedback is a large contributor to the net total cloud feedback and its multimodel variability in modern GCMs[1]. As a result, it greatly influences the magnitude of model climate sensitivity[2–4] (Fig. 1f). Given the evidence presented here, we assess the implications of possible smaller tropical low-cloud feedbacks for the ECS of Earth's climate to increasing CO_2 emissions. Assuming for illustration purposes that the influence of low-cloud feedback on overall ECS in state-of-the-art GCMs participating in the 6th Coupled Model Intercomparison Project (CMIP6) (Fig. 1f) is representative of the real-world relationship between the two, we estimate a plausible real-world ECS as a function of the observationally inferred low-cloud feedbacks from different hypothetical scenarios of SST and EIS pattern change in a climate warming (Supplementary Fig. 11), i.e., historical 40- and 60-year trends, GCM-simulated abrupt-4xCO2, and GCM-simulated +4K. Should the historical SST and EIS pattern trends (for either 1979-2018 or 1959-2018) persist, our observational constraint would suggest an ECS of 3.47 ± 0.33 K and 3.73 ± 0.36 K as opposed to 3.82 ± 0.38 K for a warming pattern similar to the CMIP6 mean abrupt-4xCO2 climate change. These estimates do not represent the true ECS but rather provide an estimate of the possible change in ECS related to the SST/EIS pattern effect on low-cloud feedback. Additionally, we address the possible effect of a biased tropical low-cloud feedback on ECS below.

The 1.5-4.5 K spread in model ECS has remained fairly constant since the first multi-model assessment[26]. However, the new GCM generation includes a number of models with even larger ECS[27], which is largely attributed to contributions from low-cloud feedbacks, mostly at middle latitudes and partly in the tropics. A simple comparison of the relationship between low-cloud feedbacks and ECS of the previous and current GCM generations suggests that an increase in tropical low-cloud feedbacks explains up to a third of the ECS increase (Supplementary Fig. 11), consistent with a more detailed analysis[27]. Furthermore, our observationally inferred estimate of low-cloud feedback for an abrupt-4xCO2 climate scenario indicates that both high-ECS and low-ECS CMIP6 models simulate unrealistic tropical low-cloud feedback, suggesting an intermediate ECS as more plausible (Fig. 5). The high-ECS models produce low-cloud feedback two times larger than the observationally constrained inference (0.56 ± 0.15 $Wm^{-2}K^{-1}$, Fig. 5a). We hypothesize that this occurs because high-ECS models simulate too many Sc-like clouds in regions dominated by Cu[18], therefore generating a stronger response of low clouds to short-term surface warming, and these clouds might also be too sensitive to climate warming[19]. On the contrary, low-ECS models predict a near-zero feedback on average, resulting from large compensating areas of negative and positive feedbacks (Fig. 5b), because they likely wrongly predict only a small decrease or an increase of low-cloud amount in response to global warming[19] (which are manifested in partial derivative errors), besides possibly underestimating the amount of Sc clouds[19], therefore generating a smaller response of low clouds to surface warming. Unfortunately, evaluating the separate GCM Sc and Cu cloud feedbacks is impossible since their respective cloud fractions are not reported in the CMIP archive.

Using our new method in conjunction with an abrupt-4xCO2 SST and EIS pattern change scenario in subsidence regimes over the tropical oceans from CMIP models, we find an observationally inferred tropical low-cloud feedback (0.56 ± 0.15 $Wm^{-2}K^{-1}$) that is two times smaller and with a five times narrower range than a previous multi-observational analysis estimate[8]. However, if the historical 40-year SST and EIS pattern trends persist in the future, our observational constraint suggests a 2.33 times smaller tropical low-cloud feedback in subsidence regimes (0.24 ± 0.12 $Wm^{-2}K^{-1}$) associated with a moderate ECS (3.47 ± 0.33 K), contrary to that in many GCMs (half of which have an ECS larger than 3.89 K). The magnitude of the ECS will be partly determined by whether the tropical Pacific Ocean begins to warm more rapidly in the east than in the west in the coming decades, as models predict, contrary to what it has been doing over the past 60 years[15,16] (Fig. 3), which models cannot replicate[5]. Additional important contributors to the strength of the tropical low-cloud feedback, and therefore the ECS, include the Sc-Cu relative presence in a given location and their sensitivity to controlling factors. Consequently, we argue that to improve predictions of future climate warming, model development should focus on how to correctly simulate the observed historical SST pattern trend and on improving the separate response of Cu and Sc clouds to SST and EIS variations along with their geographical distributions. To this end, the Cu and Sc cloud fractions should be added to the list of mandatory CMIP variables to further understand and evaluate GCM low-cloud feedbacks using the observations and method presented here.

References

1. Zelinka, M. D., Zhou, C. & Klein, S. A. Insights from a refined decomposition of cloud feedbacks. *Geophys. Res. Lett.* **43**, 9259–9269 (2016).
2. Bony, S. & Dufresne, J. L. Marine boundary layer clouds at the heart of tropical cloud feedback uncertainties in climate models. *Geophys. Res. Lett.* **32**, L20806 (2005).
3. Vial, J., Dufresne, J. L. & Bony, S. On the interpretation of inter-model spread in CMIP5 climate sensitivity estimates. *Clim. Dyn.* **41**, 3339–3362 (2013).

4. Caldwell, P. M., Zelinka, M. D., Taylor, K. E. & Marvel, K. Quantifying the sources of intermodel spread in equilibrium climate sensitivity. *J. Clim.* **29**, 513–524 (2016).
5. Wyant, M. C., Bretherton, C. S., Rand, H. A. & Stevens, D. E. Numerical Simulations and a Conceptual Model of the Stratocumulus to Trade Cumulus Transition. *J. Atmos. Sci.* **54**, 168–192 (1997).
6. Qu, X., Hall, A., Klein, S. A. & Caldwell, P. M. On the spread of changes in marine low cloud cover in climate model simulations of the 21st century. *Clim. Dyn.* **42**, 2603–2626 (2014).
7. Brient, F. & Schneider, T. Constraints on climate sensitivity from space-based measurements of low-cloud reflection. *J. Clim.* **29**, 5821–5835 (2016).
8. Klein, S. A., Hall, A., Norris, J. R. & Pincus, R. Low-Cloud Feedbacks from Cloud-Controlling Factors: A Review. *Surv. Geophys.* **38**, 1307–1329 (2017).
9. Vial, J., Bony, S., Stevens, B. & Vogel, R. Mechanisms and Model Diversity of Trade-Wind Shallow Cumulus Cloud Feedbacks: A Review. *Surv. Geophys.* **38**, 1331–1353 (2017).
10. Bretherton, C. S. Insights into low-latitude cloud feedbacks from high-resolution models. *Philos. Trans. R. Soc. A Math. Phys. Eng. Sci.* **373**, (2015).
11. Narenpitak, P. & Bretherton, C. S. Understanding Negative Subtropical Shallow Cumulus Cloud Feedbacks in a Near-Global Aquaplanet Model Using Limited Area Cloud-Resolving Simulations. *J. Adv. Model. Earth Syst.* 1600–1626 (2019) doi:10.1029/2018MS001572.
12. Cesana, G., Del Genio, A. D. & Chepfer, H. The Cumulus And Stratocumulus CloudSat-CALIPSO Dataset (CASCCAD). *Earth Syst. Sci. Data Discuss.* **2667637**, 1–33 (2019).
13. Wood, R. & Bretherton, C. S. On the relationship between stratiform low cloud cover and lower-tropospheric stability. *J. Clim.* **19**, 6425–6432 (2006).
14. Myers, T. A. & Norris, J. R. Reducing the uncertainty in subtropical cloud feedback. *Geophys. Res. Lett.* **43**, 2144–2148 (2016).
15. Seager, R. *et al.* Strengthening tropical Pacific zonal sea surface temperature gradient consistent with rising greenhouse gases. *Nat. Clim. Chang.* **9**, 517–522 (2019).
16. Coats, S. & Karnauskas, K. B. Are Simulated and Observed Twentieth Century Tropical Pacific Sea Surface Temperature Trends Significant Relative to Internal Variability?

Geophys. Res. Lett. **44**, 9928–9937 (2017).

17. Qu, X., Hall, A., Klein, S. A. & Deangelis, A. M. Positive tropical marine low-cloud cover feedback inferred from cloud-controlling factors. *Geophys. Res. Lett.* **42**, 7767–7775 (2015).
18. Nuijens, L., Medeiros, B., Sandu, I. & Ahlgrimm, M. The behavior of trade-wind cloudiness in observations and models: The major cloud components and their variability. *J. Adv. Model. Earth Syst.* **7**, 600–616 (2015).
19. Cesana, G. *et al.* Evaluating models' response of tropical low clouds to SST forcings using CALIPSO observations. *Atmos. Chem. Phys.* **19**, 2813–2832 (2019).
20. Andrews, T. & Webb, M. J. The dependence of global cloud and lapse rate feedbacks on the spatial structure of tropical pacific warming. *J. Clim.* **31**, 641–654 (2018).
21. Zhou, C., Zelinka, M. D. & Klein, S. A. Impact of decadal cloud variations on the Earth's energy budget. *Nat. Geosci.* **9**, 871–874 (2016).
22. Richter, I. Climate model biases in the eastern tropical oceans: Causes, impacts and ways forward. *Wiley Interdiscip. Rev. Clim. Chang.* **6**, 345–358 (2015).
23. Marvel, K., Pincus, R., Schmidt, G. A. & Miller, R. L. Internal Variability and Disequilibrium Confound Estimates of Climate Sensitivity From Observations. *Geophys. Res. Lett.* **45**, 1595–1601 (2018).
24. Tselioudis, G., Rossow, W., Zhang, Y. & Konsta, D. Global weather states and their properties from passive and active satellite cloud retrievals. *J. Clim.* **26**, 7734–7746 (2013).
25. Bony, S., Dufresne, J. L., Le Treut, H., Morcrette, J. J. & Senior, C. On dynamic and thermodynamic components of cloud changes. *Clim. Dyn.* **22**, 71–86 (2004).
26. Knutti, R., Rugenstein, M. A. A. & Hegerl, G. C. Beyond equilibrium climate sensitivity. *Nat. Geosci.* **10**, 727–736 (2017).
27. Zelinka, M. D. *et al.* Causes of Higher Climate Sensitivity in CMIP6 Models. *Geophys. Res. Lett.* **47**, 1–12 (2020).

Methods

Interannual low cloud response to surface warming forcings

We calculate the interannual relationship between SST, EIS and low cloud fraction following the method used in Cesana et al.[19]. We focus on low clouds over the tropical oceans (between 35˚S and 35˚N) in subsidence regimes defined as having a large-scale pressure vertical velocity at 500 hPa (ω_{500}) greater than 10 hPa/day (LCC_{sub}), based on the monthly mean of three reanalysis products (Supplementary Table 2). This filtering captures most of the stratocumulus, stratocumulus-to-shallow-cumulus transition, and cumulus regions. The 10 hPa/d threshold ensures that we select subsidence regimes only and almost perfectly encompasses areas where the height at which the CALIPSO lidar attenuates is less than 2 km (see Supplementary Fig. 2 of Cesana et al.[19]). Thus the lidar is able to detect virtually all low clouds (cloud top below ~ 3 km) in these regions with little obscuration from higher clouds. As a result, these interannual relationships take into account the geographical variability of LCC over subsiding tropical ocean regions with the climatological seasonal cycle removed.

After removing all grid boxes where ω_{500} is lower than 10 hPa/d, we use the monthly means of LCC and monthly anomalies of SST and EIS based on 10 years (120 months between January 2007 and December 2016) of three SST datasets and three reanalysis-based EIS products (Supplementary Table 2) as well as CALIPSO-CASCCAD observations for LCC_{sub} and each cloud type, all interpolated to a 2.5˚x2.5˚ grid. We then compute a multilinear regression between LCC_{sub} and the $SST_{sub,anom}$ and $EIS_{sub,anom}$ quantities to obtain the change in LCC per K of SST or EIS change, represented as the partial derivatives with respect to SST and EIS, i.e., $\frac{\partial LCC}{\partial SST}$ and $\frac{\partial LCC}{\partial EIS}$. This process is repeated for each of the nine possible combinations of the three EIS and three SST datasets, resulting in nine different estimates of the partial derivatives.

We can then compute the LCC partial derivatives for each CASCCAD cloud-type category: Sc, broken Sc, Cu under Sc, Cu with stratiform outflow, and Cu (Supplementary Fig. 5). For the purpose of this study, we define LCC_{type} (and CRE_{type}), where type is either Sc or Cu, as the cloud fraction (and CRE) in a gridbox dominated by the Sc or Cu type. To this end, we mask out (set to 0) the CASCCAD LCCs and CERES-EBAF CREs in regions where other cloud types dominate for each month, using a ratio between the cloud type fraction and the total low-cloud fraction, $\frac{LCC_{type}}{LCC}$, referred to as the Sc/(Sc+Cu) ratio (see Fig. 1c). The Cu type consists only of the Cu category of CASCCAD while the Sc type includes all clouds with a stratiform component, i.e.,, Sc, broken Sc, Cu under Sc, Cu with stratiform outflow and other clouds (see Cesana et al.[12] for details about cloud types).

To obtain the total derivative of LCC with respect to SST for a given low cloud type, we simply compute a linear regression instead of a multilinear regression, which we express as in Eq. 2.

SST and EIS pattern changes and trends

We make an observationally based inference of low-cloud feedback *dCRE/dT* as the sum of changes due to EIS and SST pattern changes of possible future climate scenarios multiplied by the partial derivatives of the cloud fraction of each low-cloud type (i.e., Sc and Cu) with respect to EIS and SST derived from the CASCCAD dataset ($\frac{\partial LCC}{\partial SST}$ and $\frac{\partial LCC}{\partial EIS}$). In this study, we use four possible future climate scenarios: two based on common GCM future climate experiments, an abrupt quadrupling of CO2 (abrupt-4xCO2) and a uniform 4 K SST increase (amip-p4K, referred to as uniform +4K), and two based on observed historical changes (the past 40 and 60 years). For the abrupt-4xCO2 and uniform +4K GCM scenarios, as in Eq. 3 below, we compute the SST and EIS changes as the difference between the mean of years 121-150 of the climate change experiments (abrupt-4xCO2 and uniform +4K) minus that of the control (piControl and amip experiments, respectively) in subsidence regimes (as defined in the previous section) divided by the difference of the global mean surface temperature between the two experiments. For the abrupt 4xCO2 experiment, we use 40 CMIP6 models while we use 10 CMIP6 models for the uniform +4K GCM experiment, based on data availability (see Supplementary Table 1). For the historical climate scenarios, we compute yearly trends of SST and EIS from observations and reanalyses (see list in Supplementary Table 2) normalized by the trend of change in global mean surface temperature over the same time period using the observed past 40 or 60 years. These trends illustrate what the low-cloud feedback would be if the historical SST and EIS pattern trends were to continue over the next few decades. To determine the yearly trends, we compute annual means of SST and EIS and subtract the global annual mean over the whole period of time (either 1979-2018 or 1959-2018) from each individual year to get the yearly anomaly and then normalize by the anomaly of the global mean surface temperature to obtain a trend of SST and EIS by degree of global mean surface temperature change. The patterns presented in Fig. 3 represent the average of all the models, observations and reanalyses available. Note that for the EIS trend over the 60-year period, we only use two reanalysis.

Observationally inferred SW low-cloud feedback

To compute observationally inferred SW low-cloud feedback, we first assume that the change in SW CRE in subsidence regimes over the tropical oceans is primarily driven by the change in LCC[6,8,14,19]. We can therefore re-construct the low-cloud feedback using Eq. 1 and the sensitivity of SW CRE to LCC to convert the LCC change into a cloud feedback as:

$$\frac{dCRE}{dT} = \frac{dCRE}{dLCC}\left(\frac{\partial LCC}{\partial SST}\frac{dSST}{dT} + \frac{\partial LCC}{\partial EIS}\frac{dEIS}{dT}\right) \quad (3)$$

where the dCRE/dLCC coefficient is the interannual CRE change with respect to LCC obtained by linearly regressing monthly CREs from CERES with LCCs from CASCCAD in subsidence regimes –to ensure that the effect of high clouds is negligible– over the tropical oceans following the method described above (see also Cesana et al.[19]).

Since the partial derivatives of Sc and Cu cloud types with respect to SST and EIS are different (Fig. 2 and Supplementary Fig. 5), we must further estimate the contribution of each cloud type separately in Eq. 4 and add them up. However, this method assumes that the partial derivatives of Sc and Cu are constant in space across the tropics and therefore neglects the effect of the relative presence of Sc and Cu in a given location. In reality, the partial derivatives of LCC with respect to SST and EIS actually vary depending on how many Sc or Cu clouds are present in specific regions. In regions dominated by Cu clouds, the partial derivative of Sc clouds is very small, having therefore a relatively small impact on the cloud change compared to its Cu counterpart, and vice-versa in regions dominated by Sc (see Figs. S8 and S9). To represent the radiative effect of each type of cloud depending on its relative presence in a given grid box, we weigh the partial derivatives of Sc and Cu clouds by the Sc/(Sc+Cu) ratio in each 2.5x2.5 grid box as:

$$\frac{dCRE}{dT} = \sum_{type=1}^{2}\frac{dCRE_{type}}{dLCC_{type}}\left(\frac{\partial LCC_{type}}{\partial SST}\frac{dSST}{dT} + \frac{\partial LCC_{type}}{\partial EIS}\frac{dEIS}{dT}\right)\frac{LCC_{type}}{LCC} \qquad (4)$$

Using a linear weight between the partial derivative values in their dominating and non-dominating regions (Supplementary Fig. 1) as defined by the Sc/(Sc+Cu) ratio (i.e., where $\frac{LCC_{type}}{LCC}$ is either greater or smaller than 50%), as presented in Eq. 7, gives almost identical results (not shown):

$$\frac{dCRE}{dT} = \sum \frac{dCRE_{type}}{dLCC_{type}} \left(\frac{\partial LCC_{type}}{\partial SST} X_{sst} \frac{dSST}{dT} + \frac{\partial LCC_{type}}{\partial EIS} X_{EIS} \frac{dEIS}{dT} \right) \frac{LCC_{type}}{LCC} \qquad (5)$$

where $X_Y = \frac{\frac{\partial LCC_{type,type}}{\partial Y} - \frac{\partial LCC_{type,other}}{\partial Y}}{100} \frac{LCC_{type}}{LCC}, \quad (6)$

Y is either SST or EIS, and $\frac{\partial LCC_{type,type}}{\partial Y}$ and $\frac{\partial LCC_{type,other}}{\partial Y}$ are the partial derivatives computed for each type of cloud in their dominating region (i.e., where $\frac{LCC_{type}}{LCC}$ is greater than 50%) and non-dominating regions (i.e., where $\frac{LCC_{type}}{LCC}$ is smaller than 50%), respectively.

Ignoring the effect of the relative presence of Sc and Cu clouds[8] may result in an overestimate of the inferred low-cloud feedback by more than a factor two (left vs. right panels of Supplementary Fig. 10), especially in the trade-wind regions where the sensitivity of low clouds to surface warming is relatively small. This is because almost no Sc clouds form in the trade-wind regions in the real world (Fig. 1c), despite the tendency of many models to make significant Sc there. In summary, errors in the spatial patterns of SST trend, Sc coverage, and Cu coverage all have the potential to cause errors in model-predicted ECS.

GCM SW low-cloud feedbacks

Most of the tropical cloud feedback comes from the shortwave (SW) effect of low clouds[1,27], thus we focus on the SW low-cloud feedbacks here. For the abrupt-4xCO2 GCM experiments, we compute the “actual” cloud feedback simulated by each of the 40 CMIP6 models (Supplementary Table 1) as the change in SW CRE per unit change in global mean surface temperature[2], where the CRE is the difference between clear-sky and all-sky top of the atmosphere flux. To do so, we first interpolate the model monthly outputs to a 2.5˚x2.5˚ grid and we then compute the difference between the mean SW CRE of years 121-150 of the climate change experiments minus that of the control in subsidence regimes (as defined in the method above) divided by the difference of the global mean surface temperature between the two experiments in subsidence regimes as shown in the following equation:

$$\frac{dCRE_{GCM}}{dT} = \left(\frac{1}{n+1-i}\sum_{i}^{n} CRE_{warm} - \frac{1}{n+1-i}\sum_{i}^{n} CRE_{ctrl}\right) \Big/ \left(\frac{1}{n+1-i}\sum_{i}^{n} T_{warm} - \frac{1}{n+1-i}\sum_{i}^{n} T_{ctrl}\right) \quad (7)$$

Where i =121 and n = 150, CRE is the SW CRE averaged over the tropical oceans in regimes of subsidence, warm means the climate change experiments (abrupt-4xCO2), and ctrl means the pre-industrial control run (piControl). Using the last 30 years of the simulation captures the essence of the long-term feedback[28] without having to perform the regression analysis of the entire 150-year period (not shown).

Using this approach to quantify the GCM low cloud feedback gives results that are almost identical to using a radiative kernel method[1,29] and similar to a more labor-intensive method[28] (such as the partial radiative perturbation) in this case because for low clouds over the tropical oceans, non-cloud feedbacks and the LW component of cloud feedback are very small[30].

Uncertainty analysis

Since the low cloud feedback is the sum of the Sc and Cu cloud feedbacks, its uncertainty is the sum of the absolute errors of Sc and Cu cloud feedbacks in quadrature such as:

$$\delta\frac{dCRE}{dT} = \sqrt{\left(\frac{dCRE_{Sc}}{dT}\right)^2 + \left(\frac{dCRE_{Cu}}{dT}\right)^2} \quad (8)$$

Following Eq. 6, $dCRE_{Sc}/dT$ and $dCRE_{Cu}/dT$ can be expressed as:

$$\frac{dCRE_{type}}{dT} = \frac{dCRE_{type}}{dLCC_{type}}\frac{LCC_{type}}{LCC}\frac{\partial LCC_{type}}{\partial SST}\frac{dSST}{dT} + \frac{dCRE_{type}}{dLCC_{type}}\frac{LCC_{type}}{LCC}\frac{\partial LCC_{type}}{\partial EIS}\frac{dEIS}{dT} \quad (9)$$

where the uncertainty of $dCRE_{type}/dLCC_{type}$ is negligible and dSST/dT and dEIS/dT are constants.

Therefore, the uncertainty $\delta dCRE_{type}/dT$ only comes from $\partial LCC_{type}/\partial SST$, $\partial LCC_{type}/\partial EIS$ and LCC_{type}/LCC and can be added in quadrature such as:

$$\delta\frac{dCRE_{type}}{dT} = \sqrt{\left(\frac{dCRE_{type}}{dLCC_{type}}\frac{LCC_{type}}{LCC}\frac{dSST}{dT}\delta\frac{\partial LCC_{type}}{\partial SST}\right)^2 + \left(\frac{dCRE_{type}}{dLCC_{type}}\frac{LCC_{type}}{LCC}\frac{dEIS}{dT}\delta\frac{\partial LCC_{type}}{\partial EIS}\right)^2 + \left(\left[\frac{dSST}{dT}\frac{\partial LCC_{type}}{\partial SST} + \frac{dEIS}{dT}\frac{\partial LCC_{type}}{\partial EIS}\right]\frac{dCRE_{type}}{dLCC_{type}}\delta\frac{LCC_{type}}{LCC}\right)^2} \quad (10)$$

We determine $\delta\partial LCC_{type}/\partial SST$ and $\delta\partial LCC_{type}/\partial EIS$ using the 10-90% confidence interval over the nine different observational estimates of the partial derivatives (i.e., combination of the three SST and three EIS datasets), which corresponds to 1.645 times one standard deviation. Note that using a 10-90% confidence interval from the bilinear regression of the partial derivatives does not change the results. For $\delta LCC_{type}/LCC$, we use the 10-90% confidence interval over the standard deviation of the annual mean (using 10 years).

Equilibrium climate sensitivity estimates

The GCM ECS values used in this study are computed using the Gregory et al.[31] method from 150 years of abrupt-4xCO2 and piControl runs. The global annual mean anomalies of TOA net radiation are regressed against the annual mean anomalies of global mean surface air temperature. Then the x-intercept of the line is divided by two to provide an estimate of the ECS. All the ECS estimates come from an updated version of Supplementary Table 1 in Zelinka et al.[27] except for TaiEMS1 and KACE-1-0-G, which we computed ourselves using the same method.

Finally, we use the relationship between ECS and low-cloud feedback in CMIP6 models (Fig. 1f and CMIP5 models in Supplementary Fig. 11) to derive an observationally constrained ECS from our observationally inferred low-cloud feedback. The uncertainty comes from the 10-90 % confidence interval of the best-fit regression between CMIP6 low-cloud feedbacks and ECS as well as the uncertainty estimates of the observationally inferred low-cloud feedback (see uncertainty analysis). However, it does not include uncertainty from other feedbacks not considered in our study.

References

28. Andrews, T., Gregory, J. M. & Webb, M. J. The dependence of radiative forcing and feedback on evolving patterns of surface temperature change in climate models. *J. Clim.* **28**, 1630–1648 (2015).

29. Soden, B. J. *et al.* Quantifying climate feedbacks using radiative kernels. *J. Clim.* **21**, 3504–3520 (2008).

30. Shell, K. M., Kiehl, J. T. & Shields, C. A. Using the radiative kernel technique to calculate climate feedbacks in NCAR's Community Atmospheric Model. *J. Clim.* **21**, 2269–2282 (2008).

31. Gregory, J. M. *et al.* A new method for diagnosing radiative forcing and climate sensitivity. *Geophys. Res. Lett.* **31**, 2–5 (2004).

Data availability

The CALIPSO-GOCCP CASCCAD statistical datasets (Cesana et al.[2]) can be downloaded from the GISS website (https://data.giss.nasa.gov/clouds/casccad/). CERES-EBAF 4.0 SW TOA fluxes were downloaded from the CERES website (https://ceres.larc.nasa.gov/). The CMIP6 GCMs outputs were downloaded from both the ESGF (https://esgf-node.llnl.gov/search/cmip6/) and climserv websites (https://climserv.ipsl.polytechnique.fr/). ERA5 files were downloaded from climserv. HadISST1.1 files were downloaded from https://www.metoffice.gov.uk/hadobs/hadisst/. ERSSTv5 files were downloaded from the NOAA national centers for environmental information website (https://www1.ncdc.noaa.gov/pub/data/cmb/ersst/v5/netcdf/). NCEP/DOE reanalysis2, NCEP-NCAR reanalysis1 and NOAA/CIRES/DOE 20th Century Reanalysis V3 were downloaded from the NOAA ESRL Physical Sciences Division website (http://www.esrl.noaa.gov/psd/data/).

Code availability

The codes used to produce the figures and to compute the different derivatives and feedbacks can be made available by contacting the corresponding author.

Acknowledgements

GC and AD were supported by a CloudSat-CALIPSO RTOP at the NASA Goddard Institute for Space Studies. The authors would like to thank NASA and CNES for giving access to CALIPSO and CloudSat observations, and Climserv for giving access to CALIPSO-GOCCP observations, CMIP6 model outputs and for providing computing resources. We acknowledge the World Climate Research Programme's Working Group on Coupled Modeling, which is responsible for CMIP, and we thank the climate modeling groups (listed in Supplementary Table 1 and 3) for producing and making available their model output. GC thanks Mark Richardson for proofreading the first draft of the manuscript and providing useful comments and Mark Zelinka for providing an updated version of Supplementary Table 1 of his study[27]. Finally, the authors thank the three anonymous reviewers and the editor for the helpful comments.

Correspondence and requests for materials should be addressed to GC.

Author contributions

GC designed the study and carried out the analysis with inputs from AD. GC wrote the manuscript with contributions from AD.

Competing interests statement

The authors declare that they have no conflict of interest.

Figures

Figure 1: Observed low-cloud climatology and simulated low-cloud feedback. Maps of a) low-cloud frequency of occurrence, referred to as low-cloud fraction throughout the manuscript, as observed by the version of CASCCAD that uses only CALIPSO lidar observations (CALIPSO-CASCCAD) (%, cloud top below ~ 3 km), b) shortwave cloud radiative effect as observed by CERES-EBAF ed4.0 (W/m^2), c) ratio of Sc cloud fraction to total low cloud fraction as observed by CALIPSO-CASCCAD (Sc/(Sc+Cu) ratio, %), d) "actual" low-cloud feedback in tropical ocean from 40 CMIP6 GCMs, calculated as the change in SW cloud radiative effect CRE with temperature (W/m^2/K), e) difference between low-cloud feedback of the 19 highest- and 21 lowest-ECS CMIP6 models with respect to the multimodel mean ECS (respectively high-ECS and low-ECS, see Supplementary Table 1) and f) relationship between the "actual" low-cloud feedback and ECS in CMIP6 models, all in subsidence regimes (ω_{500} > 10 hPa/day, where ω_{500} is the 500 hPa pressure vertical velocity). The solid blue line represents the 50 % iso-contour of CALIPSO-CASCCAD Sc/(Sc+Cu) ratio, which discriminates Sc- from Cu-dominated regions, while the dashed blue line is the 1 K iso-contour of the EIS from reanalysis in the left column (see Supplementary Table 2) and the CMIP6 model mean in the right column, which may be used as a proxy to delimit Sc and Cu cloud regimes when averaged over a long period of time (see Supplementary Text 1 and Supplementary Fig. 2).

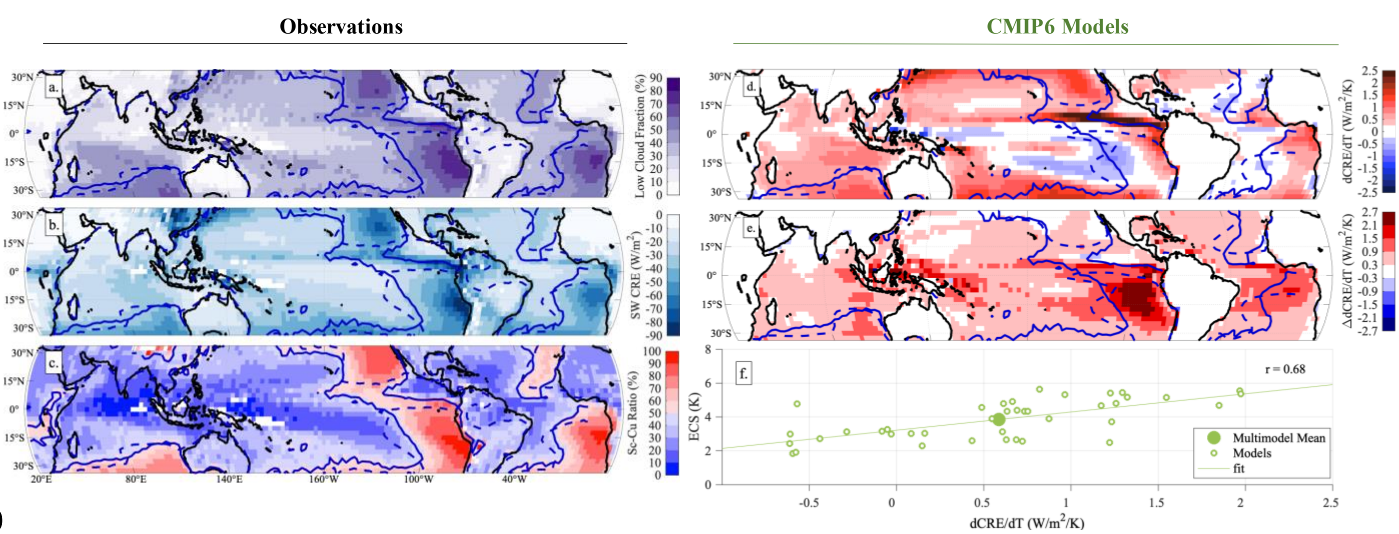

Figure 2: Observed sensitivity of low-cloud type to environmental factors (2007-2016). (a) Observed low-cloud fraction (%) in subsidence regimes over the tropical oceans (ω_{500} > 10 hPa/day) (all clouds in black, stratocumulus dominated regions in red, shallow cumuli dominated regions in blue); b) interannual low-cloud change per K of SST warming (dLCC/dSST , % K^{-1}), c) interannual low-cloud change per K of SST warming with EIS held constant (∂LCC/∂SST , % K^{-1}), d) interannual low-cloud change per K of EIS increase with SST held constant (∂LCC/∂EIS, % K^{-1}) from CALIPSO-CASCCAD and six observational and reanalysis products. The uncertainty bars correspond to the interannual mean variability for (a), and the 10-90% confidence interval using the three SST datasets for b), and three SST and EIS datasets for c) and d).

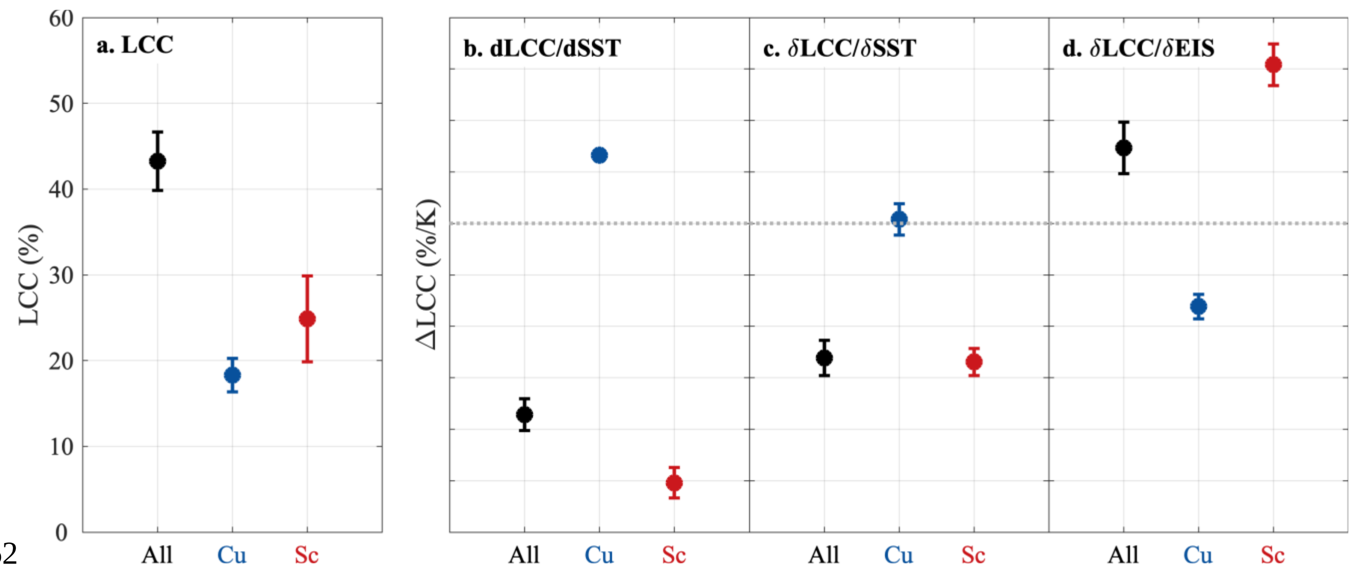

Figure 3: SST and EIS observed historical trends and simulated future changes. Maps of SST (top) and EIS (bottom) change [K/K] for different climate warming scenarios in subsidence regimes (upper left to lower right): observed historical based on the past 40 and 60 years, simulated abrupt-4xCO2 and uniform +4K. The SST and EIS pattern differences in the abrupt-4xCO2 and uniform +4K scenarios are obtained from 40 and 14 CMIP6 models (Supplementary Table 1) while the historical trends are derived from a set of observational and reanalysis products depending on availability (Supplementary Table 2). See the Methods section for details on computation of the trends.

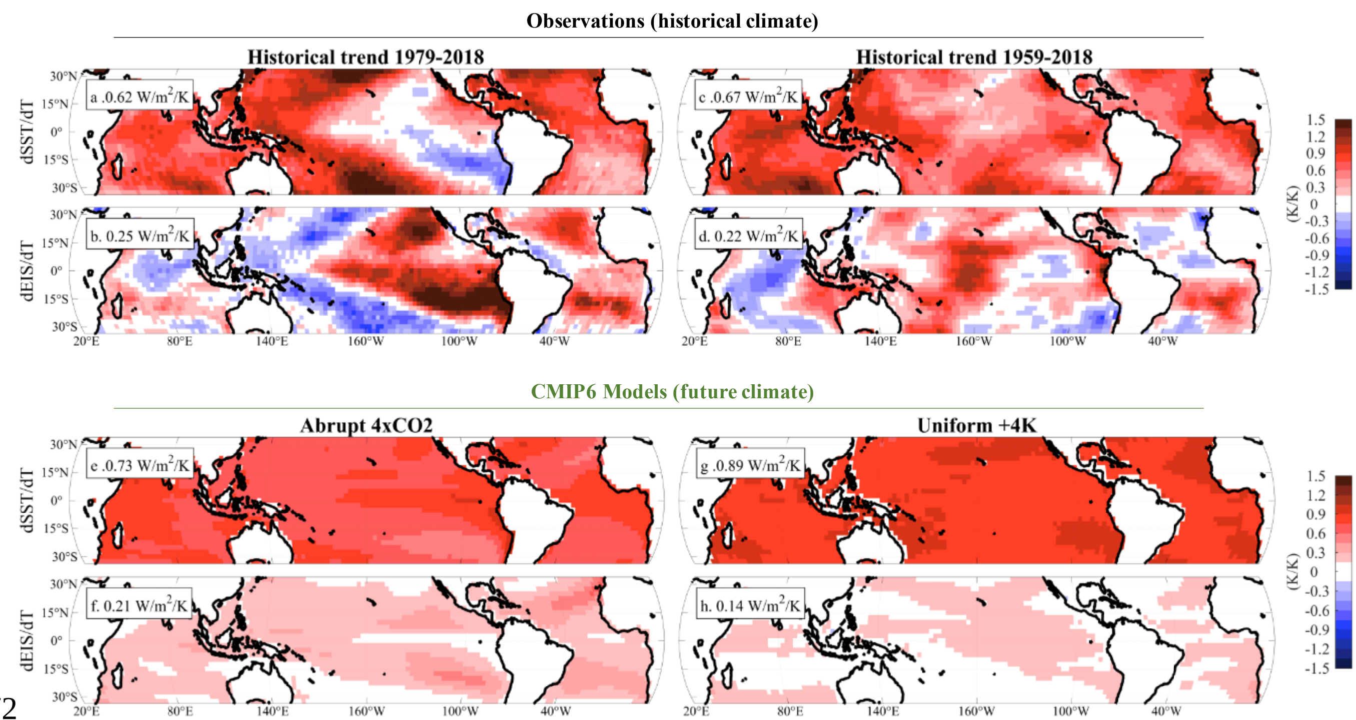

Figure 4: Observationally inferred total, Sc and Cu cloud feedback for different potential future SST pattern trends. Maps of observationally inferred (top row) total, (second row) Cu, and (third row) Sc cloud feedback ($Wm^{-2}K^{-1}$) inferred from the CALIPSO-CASCCAD-based partial derivatives and Sc/(Sc+Cu) fraction and potential future SST and EIS pattern changes from different climate warming scenarios (upper left to lower right): historical climate using the past 40 and 60-year SST and EIS pattern trends based on observations and reanalyses, and future climate using abrupt-4xCO2 and uniform +4K SST and EIS pattern changes based on CMIP6 models. Note that while the historical trends using the past 60 years produce a total feedback 15% smaller than that of an abrupt-4xCO2, its pattern is substantially different and converges to that of the historical climate using the past 40 years (see also the historical 50-year feedback in Supplementary Fig. 7).

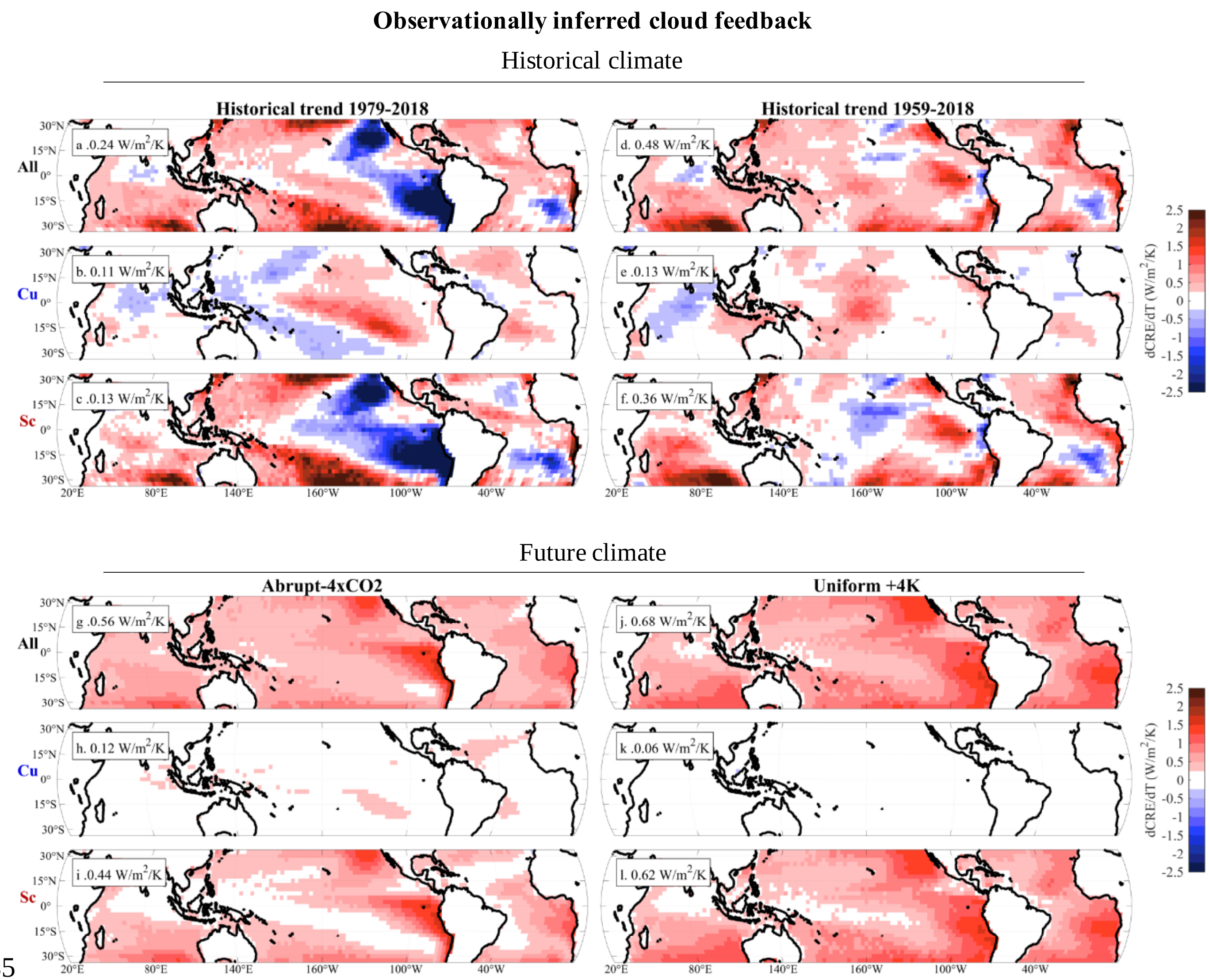

Figure 5: Simulated vs. observationally inferred low-cloud feedback. Maps of "actual" low-cloud feedbacks derived from the abrupt-4xCO2 experiments of (a) high-ECS models, (b) low-ECS models and (c) all CMIP6 models (see Supplementary Table 1), and (d) the observationally inferred feedback inferred from CALIPSO-CASCCAD-based partial derivatives and Sc/(Sc+Cu) fraction and potential future SST and EIS pattern changes from for the simulated abrupt-4xCO2 (as in Fig. 4g), in subsidence regimes.